Tight-binding theory of ZnS/CdS nanoscale heterostructures: Role of strain and *d* orbitals

J. G. Díaz, M. Zieliński,* and W. Jaskólski
Instytut Fizyki UMK, Grudziadzka 5, 87-100 Toruń, Poland

Garnett W. Bryant
National Institute of Standards and Technology, Gaithersburg, Maryland 20899-8423, USA
(Received 22 June 2006; revised manuscript received 27 September 2006; published 9 November 2006)

The electronic and optical properties of colloidal multishell ZnS/CdS nanoscale heterostructures have been studied in the framework of empirical tight-binding models. Our approach takes into account the effects of the strain caused by the large lattice mismatch at the interface between the two materials. We show that the inclusion of *d* orbitals into a minimal basis set is necessary to provide a correct description of the ZnS and CdS clads that are only a few monolayers (MLs) thick. The role of strain is also important. Strain shifts of the electron energy levels are highly dependent on the thickness of the core and shell materials. The effects of strain in the valence band are more complex. In CdS/ZnS structures, strain can change the symmetry of the ground hole state. In ZnS/CdS systems, strain lowers the energy of the ground hole state of *P* symmetry with respect to the first *S* symmetry state. Lattice relaxation also redistributes the charge densities of electron and hole states. The predicted absorption onsets resulting from our model are in good agreement with the experimental data and in better agreement with data than previous theories without strain and *d* orbitals.

DOI: 10.1103/PhysRevB.74.205309 PACS number(s): 73.21.La, 73.22.−f, 78.67.−n, 71.15.Ap

I. INTRODUCTION

Chemical growth of colloidal quantum dots enables the synthesis of extremely small multishell structures built with concentric layers of different materials, with shell thickness down to a single monolayer.[1–5] The most enticing feature of multishell nanocrystals is the flexibility to tailor their discrete spectra by sequentially cladding narrow- and wide-gap materials. In particular, cladding a narrow-gap core nanocrystal with a larger gap barrier material localizes the electron and hole states to the internal core and passivates core surface dangling bonds. This capping enhances the dot luminescence efficiency. More complicated nanoscale heterostructures (nanoheterostructures) with a core, a lower band-gap shell that acts as a well, and a high band-gap cladding layer can also be grown. In such nanodots, the optical properties are mainly controlled by the size and location of the well. Quantum-dot quantum-well (QDQW) nanostructures made of CdS/HgS/CdS have been grown and characterized.[1,6,7] HgS and CdS have similar lattice constants, which allows the fabrication of lattice-matched QDQWs. Nanoheterostructures with a large exciton binding energy and a large band gap, useful for blue-green emitting devices, can be made of material pairs like ZnS and CdS with a large lattice mismatch. The appealing applications of such nanoheterostructures as efficient, high-temperature and short-wavelength light sources has stimulated the development of their synthesis. As a result, small (2–3 nm in size) CdS and ZnS core nanocrystals, covered by one- or two-monolayer (ML)-thick shells and clads have been grown.[4]

Modeling the optical properties of multishell nanostructures with thin layers is challenging. Although effective-mass theory can predict some features of the optical spectra in reasonable agreement with the experiment,[8,9] a theory for QDQW structures that can account for atomic-scale variation in composition, such as shells that are only one monolayer thick, is required. Tight-binding (TB) theory, as an atomistic approach, allows for precise, unambiguous modeling of the dot size, shape, and composition.[7,10,11] Previously the semiempirical sp^3s^* tight-binding model including interactions up to nearest neighbors but excluding the effects of lattice mismatch was employed to model the optical properties of the above-mentioned ZnS/CdS heterostructures.[4,12,13] Reasonable agreement with experiment was obtained but significant differences remained.[4]

In this paper, we reinvestigate the electronic and optical properties of CdS/ZnS nanoheterostructures to extend and improve our understanding of these systems. Previous modeling of these nanoheterostructures was limited for two important reasons. First, in the previous sp^3s^* tight-binding models, a phenomenological s^* orbital was used to simulate the effects of higher bands, such as those due to *d* orbitals, on the conduction band.[14] However, suitable tight-binding models with *d* orbitals in the basis set have now been developed for II-VI semiconductors including CdS and ZnS. They provide a correct description both for the bulk band dispersions[15] and the band-gap evolution with size in homogeneous nanocrystals.[16,17] In our recent studies of the optical properties of GaAs (Ref. 18) and CdSe (Ref. 19) nanocrystals, we also showed that the inclusion of *d* orbitals in a minimal sp^3d^5 basis set is necessary for a proper description of the lower electron states, especially for small nanocrystals, i.e., in the strong confinement regime. The nanoheterostructures we investigate in this paper are built with CdS and ZnS shells and clads that are just one or two monolayers thick. Therefore the quantum confined states will be made from bulk states with *k* vectors that are away from the zone center. The sp^3d^5 tight-binding model reproduces the bulk-band curvatures near high-symmetry points better than the sp^3s^* models can and thus is needed to provide a good description of the electronic structure of systems with thin layers. For this reason, we have extended our tight-binding model to include *d* orbitals.[15,20] We show here that the inclusion of *d* orbitals significantly changes the electron and hole energy levels and

is necessary for the proper description of the optical properties of ZnS/CdS and CdS/ZnS nanoheterostrucrures.

ZnS/CdS nanoheterostructures have a large ($\approx 7\%$) lattice mismach at the ZnS/CdS interfaces. Similar lattice mismatch occurs in self-assembled InAs/GaAs quantum dots grown by the Stransky-Krastanov technique. This interfacial stress is responsible for the growth of such dots and substantially influences their electronic and optical properties.[21–23] This suggests that strain and lattice relaxation effects should also be taken into account in modeling multishell ZnS/CdS quantum dots. However, strain effects have been neglected so far in modeling ZnS/CdS heterostructures.[12,13]

Interfacial strain has been studied previously in CdTe/CdS systems. Rockenberger *et al.*[24] demonstrated by extended x-ray-absorption fine-structure experiments (EXAFS) that the smaller-lattice shell made of CdS compressed the larger-lattice core, increasing the Debye temperature of the CdTe core. The CdTe core also expands the CdS clad, softening the vibrational modes of the surface CdS. Thus a theory that provides a reliable description of optoelectronic properties in multishell nanostructures formed of components with a large mismatch should include strain and lattice relaxation effects. Here, we include strain and lattice relaxation effects in our modeling of ZnS/CdS nanostructures. This atomistic modeling adequately accounts for strain effects in multishell nanocrystals.

In this work, the electronic and optical properties of spherical ZnS/CdS, CdS/ZnS core-shell, and ZnS/CdS/ZnS QDQW systems are studied within the semiempirical sp^3d^5 model. Small uniform ZnS and CdS nanocrystals are also considered. To explain the role of d orbitals, a comparison with the results obtained in the sp^3s^* model is given. Large differences are observed between the two approaches, particularly in the description of uniform ZnS nanodots and CdS nanocrystals covered by ZnS clads. Strain effects are included in both models by means of the valence force field (VFF) approach.[25] Strain affects the electron and hole energy levels and significantly changes the degree of carrier localization in the CdS layers. Our results are compared with the available experimental data, yielding improved agreement between theoretical and experimental absorption onsets.

II. THEORY AND COMPUTATIONAL DETAILS

In our TB scheme, we begin with the atoms in the nanoheterostructure initially located on the regular zinc-blende lattice of the uniform core material. Such a uniform system exhibits enormous strain, because the atoms in clad layers that are different from the core are far from their bulk positions. To minimize the strain energy, we relax the lattice using the valence force field method.[25,26] We allow the atoms in the dot to move in any direction to achieve strain relaxation at the interfaces. The minimization of the strain energy is performed using a combination of the steepest descent and conjugate gradient techniques.[27] The lattice relaxation stops when the maximum force applied to each atom is less than 6×10^{-6} eV/nm. With the lattice relaxed and all the atoms in their new positions, the local strain tensor ϵ and strain profiles are calculated.[25] We analyze both the $\mathrm{Tr}(\epsilon)$, which represents the hydrostatic strain, and biaxial strain component $B=\epsilon_{zz}-(\epsilon_{xx}+\epsilon_{yy})/2$. These values help to understand how strain effects influence the one-particle states in quantum dots. In particular, $\mathrm{Tr}(\epsilon)$ and B can be used to estimate strain-induced confinement potentials [i.e., the spatial dependence of the modified conduction-band (CB) and hole valence-band (VB) edges in the quantum dot].

The relaxed atomic positions produce local changes of the bulk matrix elements between neighboring atoms (off-site TB parameters V_{kl}). The effects of changed bond angles are calculated using the Slater-Koster formulas;[28] the power-law scaling is used for the changed bond lengths: $V_{kl}=V_{kl}^0\left(\frac{d_{ij}^0}{d_{ij}}\right)^\kappa$, where d_{ij} is the bond length between the nearest neighbors i and j, and the superscript 0 corresponds to the unstrained values. The exponent κ is determined by fitting the ZnS and CdS volume deformation potentials under hydrostatic pressure, $a_v^\alpha=V\frac{\partial E_{gap}^\alpha}{\partial V}\big|_{V_0}$, to their experimental values, where α is an interband transition.[21] In Ref. 29, the experimental pressure (p) coefficient for the interband transition, $\Gamma_c\leftarrow\Gamma_v$, $a_p^{\Gamma_c-\Gamma_v}$, is quoted for both CdS and ZnS. $a_p^{\Gamma_c-\Gamma_v}$ is related to the volume (v) deformation potential via the bulk modulus D, $a_p^{\Gamma_c-\Gamma_v}=-\left(\frac{1}{D}\right)a_v^{\Gamma_c-\Gamma_v}$.[22] From this relation, $a_v^{\Gamma_c-\Gamma_v}=-4.93$ eV for ZnS, and $a_v^{\Gamma_c-\Gamma_v}=-2.83$ eV for CdS. In principle, κ may have different values for different off-site parameters. However, we find that in the sp^3d^5 model a single exponent, $\kappa=2.03$, for all matrix elements and both materials is sufficient to provide a reliable description of the bond-length dependence. A single exponent is sufficient because in the sp^3d^5 parametrization proposed by Sarma,[15] the hopping parameters obey the universal Harrison scaling law, ensuring transferability to the nanosystems. For the sp^3s^* parametrization of Lippens,[30] matching the experimental volume deformation potentials requires rather different exponents for the two materials [$\kappa(\mathrm{CdS})=3.78$, $\kappa(\mathrm{ZnS})=2.15$]. In the absence of more detailed experimental data on the volume deformation potentials for different interband transitions, the same exponent κ was employed for all off-site parameters.

We have used two different TB parametrizations to describe the investigated nanocrystals. In the sp^3s^* model, the parameters are taken from Ref. 30; in the sp^3d^5 model, they are taken from Ref. 15 and changed slightly to reproduce the correct bulk band gap.[31] Spin-orbit coupling was incorporated in both models by including the contribution from p orbitals, while the much smaller splittings of the excited d orbitals were neglected. The p-state splitting adds two extra parameters: $\lambda_{c(a)}$, one for cation and one for anion. λ_a is intended to reproduce the bulk zone-center splitting Δ_{SO} between the split-off band (SO) and the light- and heavy-hole (LH, HH) bands [$\Delta_{SO}(\mathrm{CdS})=80$ meV, $\Delta_{SO}(\mathrm{ZnS})=67$ meV].[32] We set the zero of the energy to the top of the highest valence band. The corresponding zinc-blende bulk band structures calculated in both models are shown in Fig. 1 and will be discussed below.

To mimic the effect of surface passivation by ligands and to eliminate spurious surface states lying inside the gap, the energies of the the sp^3 hybridized dangling bond orbitals on

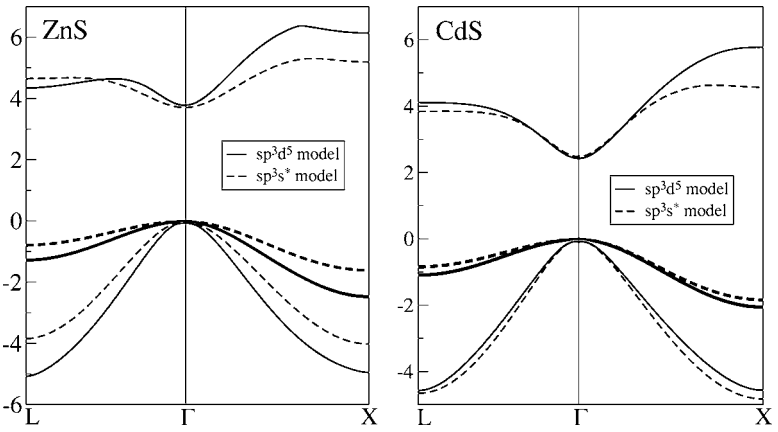

FIG. 1. Bulk band structure for ZnS and CdS along the Γ-*L* (111) and the Γ-*X* (100) directions obtained with the sp^3d^5 model (solid line) and the sp^3s^* model of Lippens (Ref. 30) (dashed line).

the surface atoms are shifted well above the conduction-band edge. The valence-band offset between ZnS and CdS is taken as 0.2 eV.[33] Once the nanocrystal structure is defined, the single-particle electron and hole eigenvalues are found by diagonalizing the TB Hamiltonian with the use of an iterative solver.

The energies and relative strengths of the electron-hole optical transitions are also estimated. The oscillator strengths are calculated by evaluating the dipole matrix elements with the use of the electron and hole TB states expanded in the atomic *s*, *p*, and *d* orbitals. The nonzero local dipole moments are evaluated by representing these orbitals in real space with Slater-type functions[34] and performing numerical integration for the radial part and exact integration for the angular part.[35] Only matrix elements between basis orbitals on the same atom site are considered. This approximation is reasonable since matrix elements between bonding orbitals on nearest neighbors are at least one order of magnitude smaller than the on-site matrix elements.[18,35]

III. RESULTS

A. ZnS and CdS nanodots

To identify the contribution of *d* orbitals in TB theory to the correct description of multishell structures, we first investigate their role in small homogeneous, uniform nanodots. The CdS and ZnS bulk band structures predicted by the sp^3s^* and sp^3d^5 models are presented in Fig. 1. The two models for CdS are similar except near *X*. For ZnS, the differences between the two models are more important. The models provide different band curvatures at high-symmetry points at the *X* and *L* edges of the Brillouin zone. Significant discrepancies are also observed in the vicinity of the Γ point, resulting in different effective masses. The CB effective mass (in electron mass units) is $m_e^*=0.49$ in the sp^3s^* model and $m_e^*=0.27$ in the sp^3d^5 parametrization. The sp^3d^5 model yields a CB effective mass in agreement with the experiment.[30] The lowest conduction band anticrosses with the higher band almost halfway between Γ and *X*. Since the higher conduction band contains important contributions from *d* orbitals in the sp^3d^5 model, the orbital character of the lowest CB changes from *s*-like to a mixture of *p*-like and *d*-like orbital character along Γ-*X*. As a result, the discrete electron states of small nanocrystals, with energies well above the bulk CB edge, will have very different character in the two TB models. Similar behavior occurs in III-V semiconductors.[18]

The extension of the orbital basis set to include *d* orbitals provides extra degrees of freedom to fit the bulk band structure to the experimental data and should yield a more realistic description of the band curvatures and the dependence of the dot energy levels on dot size. To see this, we compare in Fig. 2 the experimental absorption onset for several ZnS nanocrystals of different sizes with the predictions of the two TB models. The results obtained using the empirical pseudo-

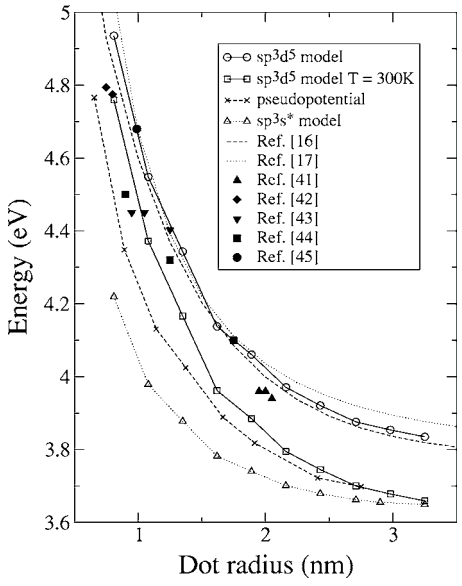

FIG. 2. Evolution of the first absorption peak in a ZnS dot vs dot radius. (a) The sp^3d^5 model, which assumes a bulk gap E_g of 3.776 eV (solid line with open circles); (b) the sp^3d^5 results shifted down by 0.176 eV to model dots at room temperature with a bulk gap $E_g=3.6$ eV (solid line with open boxes); (c) the sp^3s^* model of Lippens (Ref. 30) ($E_g=3.704$ eV) (dotted line with open triangles); (d) the pseudopotential results (Ref. 36) (dashed line with crosses); (e) the sp^3d^5 parametrization with anion-anion interactions employed in Ref. 16 (dashed line); (f) the cation sp^3–anion sp^3d^5 parametrization with next-nearest neighbor interactions developed in Ref. 17 (dotted line). Experimental absorption onsets are shown with full symbols: triangles (Ref. 41), diamonds (Ref. 42), inverted triangles (Ref. 43), boxes (Ref. 44), dots (Ref. 45).

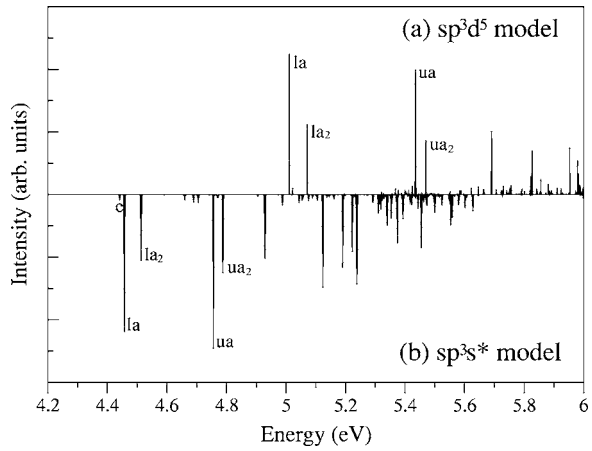

FIG. 3. Near band-edge optical spectra of a ZnS nanocrystal of radius 1.1 nm obtained with (a) the sp^3d^5 model; (b) the sp^3s^* model (Ref. 30). Transitions corresponding to the emission (e) and the intense absorption peaks (la and ua) are indicated. la_2 and ua_2 peaks label the strong transitions involving the split-off states of S and P symmetry, respectively. The atomic dipole moments used for these calculations were $\langle s|z|p_z\rangle$=0.110 nm (Zn), 0.059 nm (S); $\langle s^*|z|p_z\rangle$=0.020 nm (Zn), 0.012 nm (S); $\langle p_z|z|d_{3z^2-r^2}\rangle$=0.019 nm (Zn), 0.009 nm (S); $\langle p_x|z|d_{zx}\rangle$=0.017 nm (Zn), 0.008 nm (S); and $\langle p_y|z|d_{yz}\rangle$=0.017 nm (Zn), 0.008 nm (S).

potential method[36] are also included.[37] In each case, we shift the lowest optically active single-particle transition energy by the exciton binding energy[37] to obtain the energy of the first absorption peak. The ZnS bulk band gap varies strongly with temperature. Our sp^3d^5 model assumes the bulk band gap to be 3.776 eV. However, at room temperature the band gap is reduced to 3.6 eV.[39] In Fig. 2, the sp^3d^5 results have been shifted down by 0.176 eV to model a room-temperature gap. The effects of inhomogeneous broadening and the experimental uncertainties concerning the size of the dots studied and the temperature at which the absorption measurements were performed are responsible for the differences between the absorption onsets cited in the literature.[41–45] Despite these uncertainties, Fig. 2 shows that the experimental absorption onsets are located in the energy region spanned by the sp^3d^5 results at room and low temperature. In contrast, the sp^3s^* model predicts absorption onsets at lower energies. Pseudopotential calculations also underestimate the energy of the first absorption peak in the whole range of the studied nanocrystal sizes. The results of our TB model are in agreement with those obtained in the framework of other sp^3d^5 TB parametrizations that include anion-anion interactions,[16,17] as shown in Fig. 2.

To check the influence of d orbitals on the optical response of ZnS quantum dots, the spectrum of a 1.1-nm radius ZnS nanocrystal has been calculated with both models. They are presented in Fig. 3. Two transitions marked as la and ua dominate the spectra. Both models assign the la peak to the transition between the ground electron state (S_e) and the first hole state of the S symmetry, whereas the ua peak involves the P electron states (P_e) and the first hole state of P symmetry. In the sp^3s^* model, the ground hole state is of P symmetry, which gives rise to a single-particle transition weakly coupled to the electron ground state. In contrast, in the sp^3d^5 model, the order between the lowest hole states of S and P symmetry is reversed and therefore the same transition, i.e., $1S_h$-$1S_e$, is the lowest active transition in absorption and emission.

The single-particle band gap for this small ZnS dot [$E_g(sp^3s^*)$=4.44 eV, $E_g(sp^3d^5)$=5.01 eV] as well as the separation between the two main absorption peaks la and ua (300 meV in the sp^3s^* model and 423 meV in the sp^3d^5 model) differ significantly between the two models. These differences are a consequence of the different effective masses predicted in the two models (see Fig. 1). Because the spin-orbit coupling and bulk splittings between the HH/LH and SO bands are included similarly in the two models, the energy separation between the $la(ua)$ peak and the $la_2(ua_2)$ transition involving the corresponding split-off state is similar in the two spectra. The larger effective masses predicted by the sp^3s^* model lead to a denser distribution of transitions. In the sp^3s^* model, the first excited electron state is approximately sixfold degenerate,[46] while in the sp^3d^5 model the degeneracy is eightfold.[47] Detailed analysis of the orbital content for the first excited electron state in the sp^3d^5 model confirms that this state is built mainly of k vectors in the vicinity of the L point, instead of the Γ point as predicted by the sp^3s^* model. These differences arise because the sp^3s^* description of electron states built from the bulk states at the edge of the Brillouin zone is not reliable because this model predicts an almost flat conduction band along $X \rightarrow W \rightarrow K \rightarrow L$-edge symmetry lines.[18]

The differences between the sp^3s^* and sp^3d^5 models for CdS nanocrystals are not so pronounced as for ZnS dots. This can be inferred from the comparison of the corresponding bulk band structures presented in Fig. 1. However, since the sizes of the nanocrystals studied in this paper are small ($\approx$3 nm in diameter), some discrepancies in the energy spectrum are still observed. In particular, the $1P_e$-$1S_e$ energy separation in a small, 3-nm-diameter CdS dot increases from 361 meV in the sp^3s^* model to 437 meV in the sp^3d^5 approximation [see Fig. 4(a)]. Electron and hole states have smaller confinement energies in the sp^3s^* approach due to the larger effective masses. The difference between the ground hole states in the two models is 67 meV [Fig. 4(b)]. As in the case of ZnS, the near-band-edge optical spectra obtained in both models are qualitatively similar. The differences arise in the energy separations between the main optically active transitions.

B. CdS/ZnS nanoheterostructures

In this section we study the effect of d orbitals and strain on the properties of CdS/ZnS nanostructures with different thicknesses of the ZnS clad. We consider first structures with an unrelaxed lattice (no strain effects included). The energy levels of the electron and hole states of S and P symmetry, involved in the transitions labeled previously as la and ua, are presented in Fig. 4 for two different ZnS clad thicknesses (in the figures, CdS/ZnS indicates a 3 nm CdS core with a 1-ML ZnS clad, CdS/ZnS:ZnS indicates a 2-ML ZnS clad). For comparison, the energy levels of the uniform CdS nan-

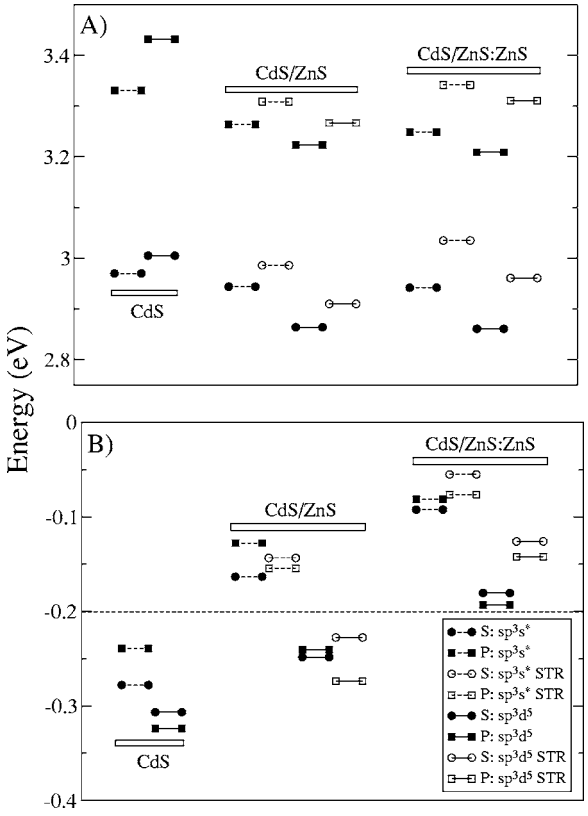

FIG. 4. Energy levels for a CdS dot and CdS/ZnS nanoheterostructures with one and two capping layers of ZnS. The CdS core is 3 nm in diameter in each case. Electron (A) and hole (B) energy levels of the first state of S (dots) and P (boxes) symmetry calculated in the sp^3s^* model (dashed lines) and the sp^3d^5 approach (solid lines) without (full symbols) and with (open symbols, STR) strain effects. The origin of energy scale is located at the top of the valence band of CdS. The dashed line marks the ZnS VB edge. The ZnS CB edge is at 3.58 eV.

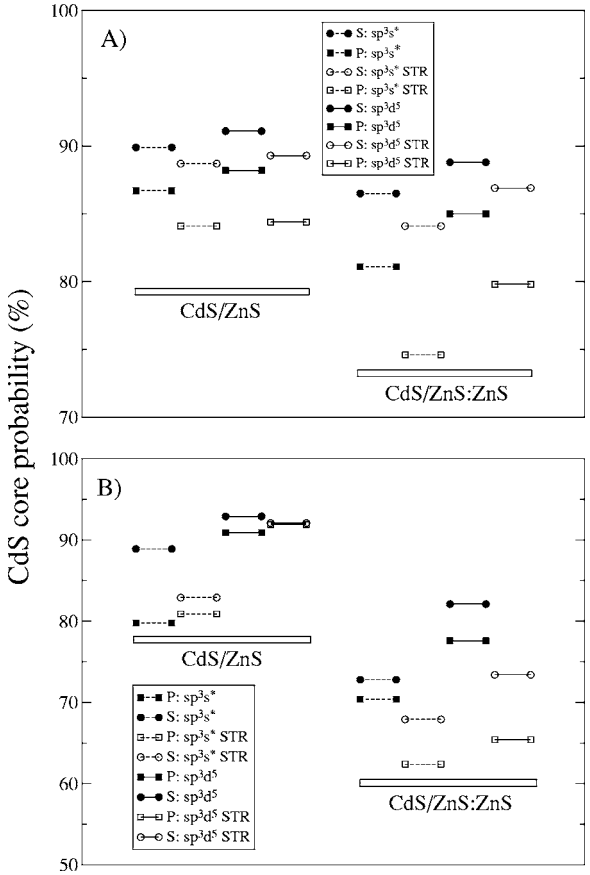

FIG. 5. Probability to be in the CdS core for the first electron (A) and hole (B) levels of S (dots) and P (boxes) symmetries. The investigated structures are those shown in Fig. 4 with lines and symbols as in Fig. 4. In the CdS/ZnS structure, the S and P hole levels calculated with the sp^3d^5 STR model overlap in the figure.

odot with a 3-nm diameter are also shown. The addition of a ZnS clad (one monolayer thick) stabilizes both the electron and hole energy levels. Stabilization of the electron levels is much more pronounced in the sp^3d^5 model, with the energy of the ground $1S_e$ state lower than in the sp^3s^* approximation. This is surprising, because in uniform nanocrystals the energy of the $1S_e$ state in the sp^3d^5 model is higher than in the sp^3s^* approach. This strong energy stabilization occurs because the electron wave functions in the sp^3d^5 model are pushed from the ZnS barrier back into the internal CdS well (the depth of the CB well increases in the sp^3d^5 model by 126 meV). As a result, the electron states are more localized to the CdS core [as shown in Fig. 5(a)] and their energies decrease. Further increase of the width of the ZnS clad does not lead to any significant changes in the electron energy spectrum.

The stabilization of the hole states by covering the CdS nanodot with a 1-ML-thick ZnS clad is stronger than for the electron states. Thus in the sp^3s^* model both the lowest S and P hole states become bound in the CdS well. The binding gets stronger when another ZnS ML is added. One can also see that the presence of an external ZnS clad reduces the separation between the lowest hole levels of S and P symmetry (sp^3s^* model) in comparison with the uniform CdS nanodot.

We now consider the effects of strain. When CdS and ZnS, with a large lattice mismatch, form a CdS/ZnS nanoheterostructure, the shorter lattice-constant ZnS external clad compresses the internal core of CdS. Conversely, the larger lattice-constant core expands the ZnS clad. The magnitude of strain induced in CdS and ZnS depends on the relative widths of the layers. When a thick CdS core is covered by a thin ZnS clad, almost the entire tensile strain accumulates in the ZnS layer. With increasing width of the ZnS shell, the strain in this shell decreases, but at the same time it increases in the internal CdS core.

In Fig. 6(a), we show the strain-modified profiles of the CB, HH, LH, and SO band edges[48] along the (001) direction, calculated for a large dot built of a CdS core of radius $6a$ (a is the lattice constant of the unrelaxed CdS core) covered by a ZnS clad of width $6a$. The corresponding unstrained confining potentials are marked with dashed lines. Here, we consider such a big dot to have enough cation atoms along the radius to clearly display the relaxed confining potentials. Similar trends concerning valence-band ordering and the band-edge shifts are observed for smaller structures. The CB edge changes due to the hydrostatic strain [$\mathrm{Tr}(\epsilon)$]: it shifts up

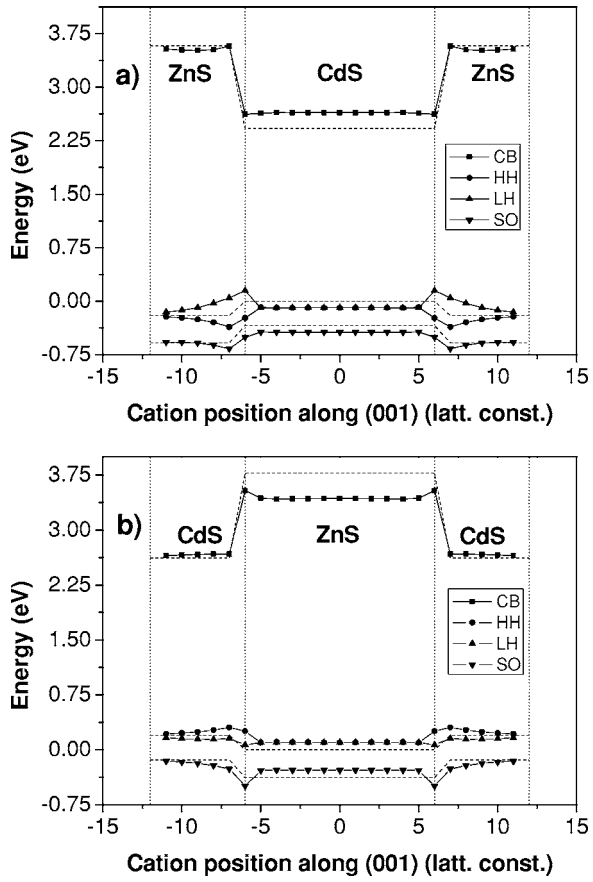

FIG. 6. Strain-modified confining potentials along the (001) direction for HH (dots), LH (triangles), SO (inverted triangles), and conduction (boxes) bands in CdS/ZnS (a), and ZnS/CdS (b) dots. The core radius is 6*a*, the external clad width is 6*a*, where *a* is the lattice constant of the unrelaxed core. The unstrained bulk band edges are shown as dashed lines.

(down) in the compressed (tensile) regions, respectively. Thus in the investigated CdS/ZnS nanocrystal, the strain induced in the CdS core shifts the electron energy levels up [Fig. 4(a)] and their charge densites in the CdS core diminish [Fig. 5(a)]. As mentioned above, the thicker ZnS clad yields stronger compression of the CdS core. As a result, when another ZnS ML is added to the clad, the strain induced destabilization of the electron energy levels doubles (from $\approx$50 meV to $\approx$100 meV). It is worthwhile to note that in both models (sp^3s^* and sp^3d^5) strain influences the electron states in a very similar way.

Strain effects in the valence band are more complex than in the conduction band. We have checked that biaxial strain component vanishes in the internal CdS core independently of the width of the CdS and ZnS layers and therefore the HH and LH bands remain degenerate there [Fig. 6(a)]. However, at the interface, biaxial strain is not zero, leading to a splitting of the HH and LH states. The LH band lowers its energy at the interface and in the thin ZnS clad, leading to formation of a light-hole well in the ZnS clad (instead of the barrier in the unstrained case). The HH barrier in the ZnS region is enhanced by the effects of biaxial strain. Additionally, the hydrostatic strain in the core shifts the upper valence bands slightly down, making the CdS well shallower. These trends help us to interpret the behavior of the discrete hole states in these quantum confined systems.

The most striking observation is that the hole state of *S* symmetry becomes the ground state when the lattice relaxes, regardless of the model employed. The *S*-type hole state is stabilized strongly by the strain. This stabilization occurs in both models (sp^3s^* and sp^3d^5) and for two different ZnS clad thicknesses. An inspection of Fig. 5(b) reveals that the charge density of the *S* state, which is initially located mainly in the CdS core, moves towards the interface, i.e., towards the LH well. This behavior is due to the significant contribution of the LH band to the character of the *S* state. When the CdS core is covered by a 1-ML-thick ZnS clad, the charge density of the more HH-like *P* state concentrates in the CdS core rather than in the ZnS HH barrier, and its energy destabilizes due to hydrostatic strain in the core. However, this trend is reversed for a 2-ML ZnS clad possibly due to a larger LH contribution to this state.

C. ZnS/CdS and ZnS/CdS/ZnS nanoheterostructures

In ZnS/CdS core-shell and ZnS/CdS/ZnS QDQW structures the electrons and holes can be confined in the potential well defined by the CdS shell. This allows the optoelectronic properties to be tailored to a larger extent because the structure of discrete energy levels is here sensitive to both the radius of the internal ZnS core and the width of CdS shell. This also implies sensitivity to the model used in the calculations.

In Fig. 7 we show the single-particle near-band-edge optical spectra for a core-shell structure with an internal ZnS core of diameter 2 nm and one ML external CdS clad. The spectra were calculated with the sp^3d^5 and the sp^3s^* models, with and without strain effects. The sp^3d^5 model predicts larger separation between the two main optical peaks (*la* and *ua*) and a smaller *la-e* shift. In the absence of lattice relaxation effects, the *ua-la* separation is 237 meV in the sp^3d^5 model, and only 154 meV in the sp^3s^* approach. On the other hand, the sp^3s^* model predicts a *la-e* shift that is twice as large as in the sp^3d^5 approach. The inclusion of strain acts in the opposite way: it reduces the *ua-la* splitting (for sp^3d^5, 168 meV; for sp^3s^*, 72 meV), and enhances the *la-e* shift (for sp^3d^5, 175 meV; for sp^3s^*, 210 meV).

In the following we analyze in detail the influence of *d* orbitals and strain effects on the optoelectronic properties of core-shell and QDQW systems. The electron energy levels calculated in different approximations for four different systems investigated are presented in Fig. 8(a). In all of these nanoheterostructures, the core radius is 1.5 a', where a' is the lattice constant of the unrelaxed ZnS core. The electron states of multishell nanostructures with a one-ML-thick CdS clad are not bound in the CdS well, i.e., they have energies above the ZnS CB edge E_{CB}=3.78 eV, according to the sp^3d^5 models. At least two CdS monolayers are needed to bind the first electron level in the CdS well. As can be observed in Fig. 8, the two TB models predict quite different positions and separations of the energy levels. This is because the CdS well is only one or two monolayers thick and

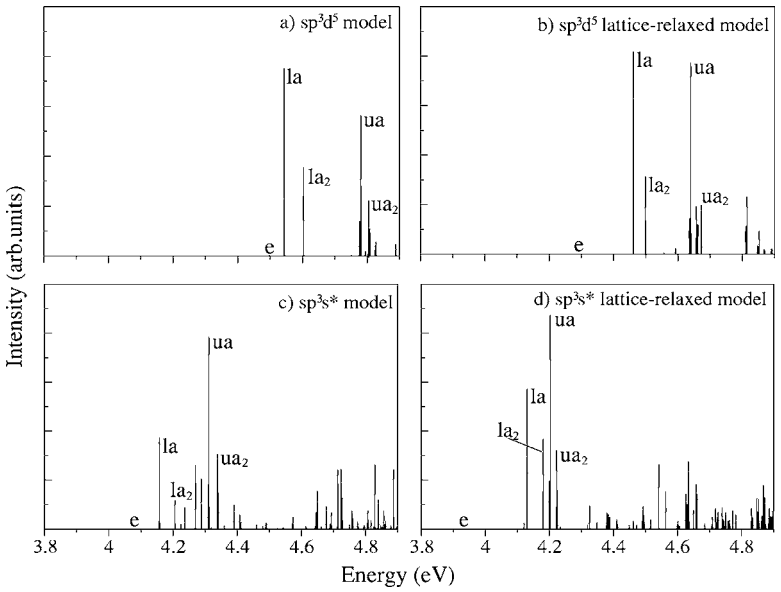

FIG. 7. Single-particle near band-edge optical spectra of ZnS/CdS nanostructure calculated with (a) sp^3d^5 model; (b) sp^3d^5 model with strain effects included; (c) sp^3s^* approach; (d) sp^3s^* approach with strain effects. The internal ZnS core diameter is 2 nm; the external CdS clad is 1 ML thick. Transitions corresponding to the emission (e) and intense absorption peaks (la, la_2, ua, and ua_2) are indicated. The same atomic dipole moments were used as in Fig. 3 for Zn and S. Atomic dipole moments for Cd are $\langle s|z|p_z\rangle = 0.127$ nm, $\langle s^*|z|p_z\rangle = 0.023$ nm, $\langle p_z|z|d_{3z^2-r^2}\rangle = 0.019$ nm, $\langle p_x|z|d_{zx}\rangle = 0.017$ nm, and $\langle p_y|z|d_{yz}\rangle = 0.017$ nm. Exciton binding energies have been neglected for sake of comparison between the two TB models.

thus the electron states are built of large k vectors, away from the bulk Γ point where the two TB models differ significantly. Additionally, the electron charge density is distributed between the CdS clad and the ZnS core. The bulk band structure of ZnS is poorly reproduced by the sp^3s^* model. However, a closer inspection of Fig. 8(a) reveals that the major effect on the electron energy levels, due to the d orbitals, is the significant destabilization of the electron levels. The only exception is the ZnS/CdS:CdS/ZnS structure, where this trend is diminished for the excited P_e state and slightly reversed for the S_e state. One should also note that the stabilization of the electron energy levels of the QDQW systems due to an external ZnS clad is much stronger in the sp^3d^5 approach. Figure 9(a) shows that in the sp^3d^5 model the charge densities of the electron states are more concentrated in the CdS well (and therefore their maxima are closer to the CdS outermost surface). This explains in part why the electron states are more sensitive to the external cladding in the sp^3d^5 approach.[49]

The energies of the hole states are strongly destabilized in the d-orbital model with respect to the sp^3s^* case. This destabilization occurs in the QDQW structures for both the relaxed and unrelaxed systems. In the ZnS/CdS core-shell structures, destabilization of the ground hole state (which is always P-type) occurs when strain effects are ignored but not when strain is included. The influence of strain effects therefore requires a detailed analysis.

In ZnS/CdS structures the internal ZnS core is stretched, while the external CdS clad is compressed. As a result, the hydrostatic strain shifts up the CB edge of the CdS clad and lowers the CB edge of the ZnS core. Therefore the CdS well becomes shallower, enhancing leakage of the electrons into the ZnS. This is well seen in Fig. 9(a) for both sp^3s^* and sp^3d^5 models. It is interesting to note that although lattice relaxation pushes the electron charge densities from the well into the ZnS barriers, the energies almost do not change. For ZnS/CdS hole states, the biaxial strain stabilizes the HH band in the CdS clad with respect to the LH band [Fig. 6(b)], reversing the order between them in comparison to CdS/ZnS dots. Thus strain should yield hole states with HH character to become more localized in the CdS well. This is the case of the ground hole state, which has P-type symmetry in all the structures considered. The strong localization in the CdS well [Fig. 9(b)] is accompanied by a large energy stabilization ($\approx$120 meV in sp^3s^* and $\approx$200 meV in sp^3d^5 model, respectively) seen in Fig. 8(b). In contrast, the lowest hole state of S symmetry is more concentrated in the ZnS region [see Fig. 9(b)]. This is seen for the ZnS/CdS structure where only the 26% (sp^3d^5)/12% (sp^3s^*) of the charge density is located in the external clad. After the lattice is relaxed, the charge density is pushed towards the external CdS clad. Thus 61% (sp^3d^5 model)/34% (sp^3s^* model) of the charge density is in the external clad (the effect is shown in Fig. 10). This severe rearrangement does not translate into substantial energy change (the energy remains unchanged in the sp^3s^* model and changes by about 50 meV in the sp^3d^5 model) due to the larger LH character of the S state. As a result, the energy separation between the lowest S and P hole levels is greatly enhanced after the lattice is relaxed, particularly in the sp^3d^5 model (see Fig. 8).

A crucial test of these models is a comparison with the experimental absorption spectra for these nanoheterostructures.[4] Inhomogeneous broadening of the spectra does not allow a resolution of individual absorption peaks, like, e.g., the la and ua peaks. However, comparisons can still be made. A comparison between experimental spectra and theory was previously addressed in the framework of the sp^3s^* model.[4,9,13,40] However, no strain effects have been considered so far. In Ref. 40 the ua peak, involving the transition between the lowest electron and hole states of P symmetry (see Figs. 3 and 7), was considered and the energy of this transition was compared with the experimental spectrum onset and the main broad absorption peak. However, in the sp^3d^5 approach the la transition can be stronger than the ua transition. Because both transitions are significant in the sp^3d^5 model (see Fig. 7), we assume that the energy range spanned by these two transitions should be compared with

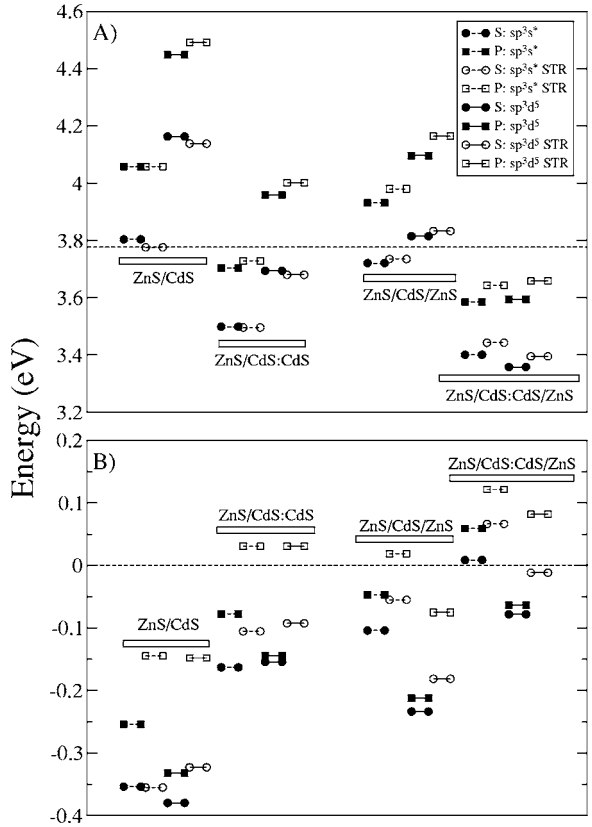

FIG. 8. ZnS/CdS core-shell and ZnS/CdS/ZnS QDQW nanostructures: Electron (A) and hole (B) energy levels of the first state of *S* (dots) and *P* (boxes) symmetry. The core radius is 1.5 a', where a' is the lattice constant of the unrelaxed ZnS core. The wells and clads are 1 or 2 MLs, as indicated. Lines and symbols are as in Fig. 4. Dashed line in (A) shows the bulk ZnS CB edge at 3.78 eV. Dashed line in (B) marks the ZnS valence-band edge. The CdS VB edge is at 0.2 eV.

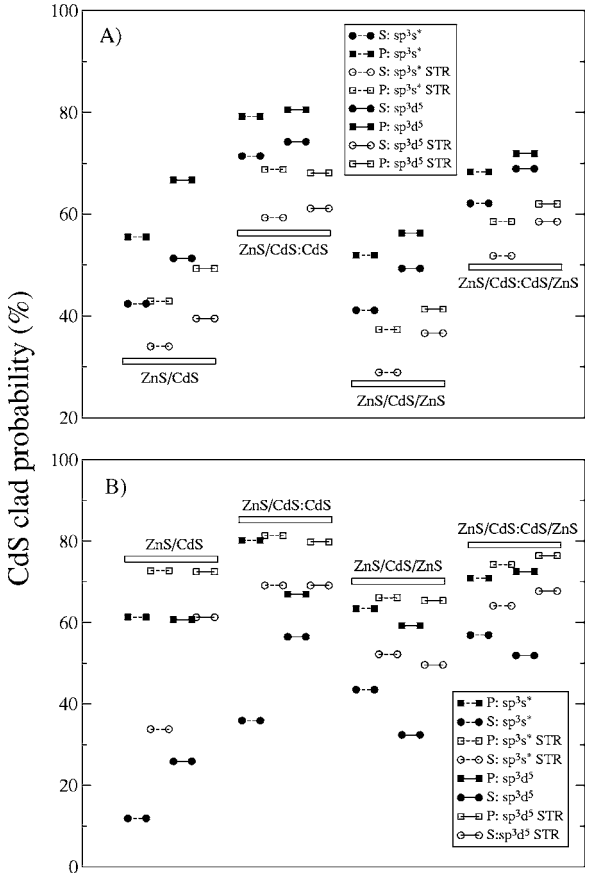

FIG. 9. Probability to be in the CdS clad for the first electron (A) and hole (B) levels of *S* (dots) and *P* (boxes) symmetries. The investigated structures are those shown in Fig. 8 with lines and symbols as in Fig. 8.

the low-energy part of experimental absorption spectra (the onset and the first broad maximum). In Fig. 11, we compare the experimental absorption spectra for the homogeneous ZnS and CdS dots and the ZnS/CdS nanoheterostructures[4] with the absorption interval defined by the *ua-la* transitions calculated in the lattice-relaxed sp^3d^5 model. The binding energy has been estimated perturbationally and subtracted from the single-particle transitions. We have assumed $\epsilon = 5.13$ for ZnS,[50] and $\epsilon = 5.5$ for CdS.[51]

For the homogeneous ZnS (labeled *z* in the figure) and CdS (c) dots, the *ua-la* interval resulting from the sp^3d^5 model defines the region between the absorption edge and its maximum in the experimental spectra (Fig. 11). In contrast, in the sp^3s^* model, the *la* wavelength for both CdS ($\lambda = 423$ nm) and ZnS ($\lambda = 314$ nm) nanocrystals is well above the absorption edge. Even assuming a larger ($\epsilon = 8.1$) dielectric constant,[52] the resulting absorption edge ($\lambda = 300$ nm) overestimates the experimental wavelength for ZnS. This suggests the necessity of including *d* orbitals in the basis set for a proper description of ZnS and CdS nanocrystals in the strong confinement regime.

The experimental absorption onset for the ZnS/CdS/ZnS QDQW (zcz) is also well-described with our model ($\lambda = 320-340$ nm). This contrasts with the sp^3s^* results ($\lambda = 345-362$ nm) which cannot reproduce the absorption maximum. The sp^3d^5 approach predicts a large blueshift when the external ZnS capping layer is removed. The theoretical absorption interval for the ZnS/CdS structure (zc) is between 298 and 311 nm. In contrast, the experimental absorption onsets for both the core-shell (zc) and the QDQW (zcz) nanodots are almost indistinguishable. This experimental evidence suggests an incomplete passivation for the ZnS/CdS structure which acts in a similar way to the external ZnS clad. The theoretical absorption onset for the core-shell material with 2 ML of CdS (zcc) defines an interval between the experimental absorption maximum and its edge. The energy interval defined by the sp^3s^* model ($\lambda = 372-383$) described only the absorption onset. In this case, the effects of surface passivation are smaller since the CdS clad is wider. However, the predicted onset for the corresponding QDQW structure with two 2 MLs of CdS in the middle well (zccz) matches the experimental absorption edge but not its maximum. The good agreement obtained between the sp^3d^5 model and experiment suggests that the CdS clad is smaller in this QDQW. For a QDQW with the CdS well and the external ZnS clad both about 1.5 ML thick (zc-cz in Fig.

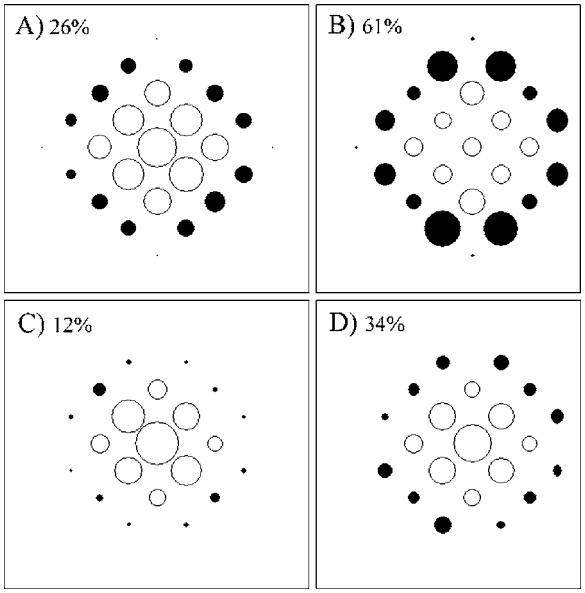

FIG. 10. Charge density for the first hole state of *S* symmetry in the ZnS/CdS nanostructure with a 1.5 *a'* ZnS core and a 1-ML CdS clad: (A) sp^3d^5 model without strain effects; (B) sp^3d^5 model including strain and lattice relaxation; (C) sp^3s^* approach without strain; (D) sp^3s^* approach with strain effects. The size of the circles quantifies charge density on anions in the dot midplane. Full circles represent atoms belonging to the external CdS clad; open circles are the atoms in the ZnS core. The total charge density in the CdS clad is indicated. Small asymmetries in the states appear because only one state from the degenerate manifold is shown.

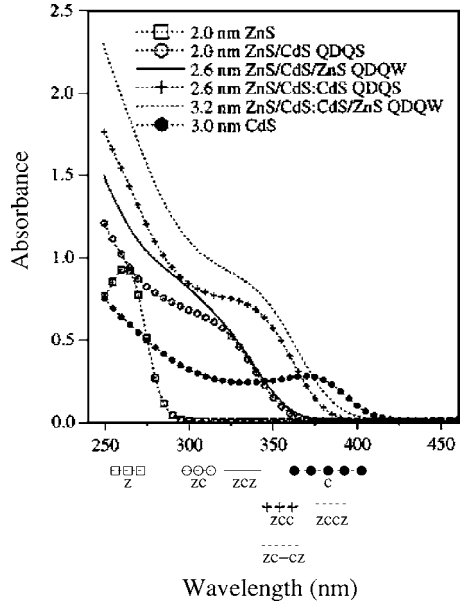

FIG. 11. Experimental absorbance for homogeneous ZnS and CdS dots, and several multishell nanostructures of Ref. 4 compared with the energy range spanned by the *ua-la* transitions calculated with the lattice-relaxed sp^3d^5 approach (horizontal lines). The diameter of each nanostructure is indicated. zc-cz labels the QDQW structure where a 1.5-ML CdS middle clad was modeled.

11), the theoretical absorption onset matches the experimental maximum.

IV. SUMMARY

We have studied the electronic structure and optical properties of small homogeneous ZnS and CdS nanocrystals and ZnS/CdS nanoheterostructures with sp^3s^* and sp^3d^5 tight-binding models. Our results show that tight-binding parametrization with *d* orbitals is necessary to describe quantitatively the absorption features of small homogeneous dots and multishell structures. The two models provide very different curvature of the bulk ZnS and CdS conduction band for energies well above the CB edge. As a result, for small nanocrystals, the sp^3s^* model underestimates the experimental effective band gap and the energy splitting between the two main absorption peaks. Particularly large differences between the two TB models are found in the case of ZnS nanodots.

We have also investigated the role of strain caused by the large mismatch at interfaces between ZnS and CdS. For core-shell CdS/ZnS structures, the hydrostatic strain makes the conduction-band CdS well shallower, concentrates the electron density in the ZnS barrier, and produces energy shifts of the electron levels that are sensitive to the ratio between the core and shell sizes. Biaxial strain affects mainly the valence bands: it leads to an attractive LH well at the interface and in the external ZnS clad, making the *S* symmetry state the ground hole state.

For ZnS/CdS core-shell and ZnS/CdS/ZnS QDQW structures, a 1-ML-thick CdS well is unable to bind the ground electron and hole states in the CdS well; the charge densities are distributed between the CdS well and the ZnS barrier(s). In contrast to CdS/ZnS systems, the biaxial strain here stabilizes the HH band in the CdS clad, which binds the first hole state of *P* symmetry in the CdS well. As a result, the separation between the two main absorption peaks is reduced. Lattice relaxation also causes substantial rearrangement of the charge density of the first hole state of *S* symmetry, moving it from the dot center to the CdS clad. Our results show that the sp^3d^5 model with strain effects taken into account provides good agreement between the predicted energy range spanned by the two main optical transitions and the experimental absorption onsets and significantly improves the theoretical understanding of these nanoheterostructures.

ACKNOWLEDGMENTS

This work was performed under the sponsorship of the U.S. Department of Commerce, NIST. The research was also financially supported by Polish Projects 1P03B15129, 3T1104326, and PZB-MIN-008/P03/2003.

*Present address: National Research Council of Canada, Ottawa, Ontario K1A OR6, Canada.

[1] A. Mews, A. Eychmüller, M. Giersig, D. Schoos, and H. Weller, J. Phys. Chem. **98**, 934 (1994).

[2] A. P. Alivisatos, Nature (London) **271**, 933 (1996).

[3] A. Mews, A. V. Kadavanich, U. Banin, and A. P. Alivisatos, Phys. Rev. B **53**, R13242 (1996).

[4] R. B. Little, M. A. El-Sayed, G. W. Bryant, and S. Burke, J. Chem. Phys. **114**, 1813 (2001).

[5] D. J. Norris and M. G. Bawendi, Phys. Rev. B **53**, 16338 (1996).

[6] M. Braun, C. Burda, and M. A. El-Sayed, J. Phys. Chem. A **105**, 5548 (2001).

[7] G. W. Bryant and W. Jaskólski, Phys. Rev. B **67**, 205320 (2003).

[8] G. W. Bryant, Phys. Rev. B **52**, R16997 (1995).

[9] W. Jaskólski and G. W. Bryant, *Proceedings of NATO ARW on the Optical Properties of Semiconductor Nanostructures*, edited by M. L. Sadowski, M. Potemski, and M. Grynberg, NATO Science Series, High Technology (Kluwer, Amsterdam, 2000).

[10] J. G. Díaz, J. Planelles, G. W. Bryant, and J. Aizpurua, J. Phys. Chem. B **108**, 17800 (2004).

[11] J. G. Díaz and J. Planelles, Langmuir **20**, 11278 (2004).

[12] G. W. Bryant and W. Jaskólski, Physica E (Amsterdam) **11**, 72 (2001).

[13] J. Pérez-Conde and A. K. Bhattacharjee, Phys. Rev. B **67**, 235303 (2003).

[14] P. Vogl, H. P. Hjalmarson, and J. D. Dow, J. Phys. Chem. Solids **44**, 365 (1983).

[15] S. Sapra, N. Shanthi, and D. D. Sarma, Phys. Rev. B **66**, 205202 (2002).

[16] S. Sapra and D. D. Sarma, Phys. Rev. B **69**, 125304 (2004).

[17] R. Viswanatha, S. Sapra, T. Saha-Dasgupta, and D. D. Sarma, Phys. Rev. B **72**, 045333 (2005).

[18] J. G. Díaz and G. W. Bryant, Phys. Rev. B **73**, 075329 (2006).

[19] J. G. Díaz and G. W. Bryant, Phys. Status Solidi C (to be published).

[20] J.-M. Jancu, R. Scholz, F. Beltram, and F. Bassani, Phys. Rev. B **57**, 6493 (1998).

[21] R. Santoprete, B. Koiller, R. B. Capaz, P. Kratzer, Q. K. K. Liu, and M. Scheffler, Phys. Rev. B **68**, 235311 (2003).

[22] L. He, G. Bester, and A. Zunger, Phys. Rev. B **70**, 235316 (2004).

[23] D. Bimberg, M. Grundmann, and N. N. Ledentsov, *Quantum Dot Heterostructures* (Wiley, New York, 1999).

[24] J. Rockenberger, L. Tröger, A. L. Rogach, M. Tischer, M. Grundmann, A Eychmüller, and H. Weller, J. Chem. Phys. **108**, 7807 (1998).

[25] C. Pryor, J. Kim, L. W. Wang, A. J. Williamson, and A. Zunger, J. Appl. Phys. **83**, 2548 (1998).

[26] T. Saito and Y. Arakawa, Physica E (Amsterdam) **15**, 169 (2002).

[27] W. H. Press, B. P. Flannery, S. A. Teukolski, and W. T. Vetterling, *Numerical Recipes* (Cambridge University Press, Cambridge, England, 1986).

[28] J. C. Slater and G. F. Koster, Phys. Rev. **94**, 1498 (1954).

[29] K. Reimann, M. Haselhoff, St. Rubenacke, and M. Steube, Phys. Status Solidi B **198**, 71 (1996).

[30] P. E. Lippens and M. Lannoo, Phys. Rev. B **39**, 10935 (1989).

[31] In Ref. 15 the electronic structure of group II-VI semiconductors was analyzed with the linearized muffin-tin orbital (LMTO) method. The LMTO provides reliable band dispersions, but it underestimates the bulk band gap. Nevertheless, the TB parameters can be slightly modified to reproduce the experimental band gap. We achieve this by shifting down the upper valence bands (heavy hole, light hole, and split off) without changing their curvatures. In practice, this translates into a change in the on-site anion p orbital (p_a) that determines the energy position of the valence bands, and the off-site $sp\sigma$ parameter that controls the band curvatures. To obtain the bulk band structure of Fig. 1, we have employed $p(a)=0.93$ eV and $sp\sigma=2.87$ eV for ZnS; and $p(a)=0.20$ eV and $sp\sigma=2.39$ eV for CdS (conventional notation for the TB parameters as in Ref. 20 is employed). Such a change preserves the chemical trends of the original LMTO-derived band structure. In particular, the orbital content of the first conduction and valence bands remain the same along L-Γ-X.

[32] In the d model, the bulk spin-orbit splittings can be reproduced by assuming $\lambda_a=42$ meV for ZnS and $\lambda_a=43$ meV for CdS. In the sp^3s^* model, $\lambda_a=28$ meV for ZnS; and $\lambda_a=30$ meV for CdS.

[33] S. H. Wei and A. Zunger, Appl. Phys. Lett. **72**, 2011 (1998).

[34] J. C. Slater, Phys. Rev. **36**, 57 (1930).

[35] S. Lee, J. Kim, L. Jönsson, J. W. Wilkins, G. W. Bryant, and G. Klimeck, Phys. Rev. B **66**, 235307 (2002).

[36] B. Zorman and R. A. Friesner, J. Chem. Phys. **118**, 5937 (2003).

[37] The exciton binding energy was estimated as in Ref. 38.

[38] L. E. Brus, J. Chem. Phys. **80**, 4403 (1984).

[39] C. Kittel, *Introduction to Solid State Physics* (Wiley, New York, 1986).

[40] G. W. Bryant and W. Jaskólski, Phys. Status Solidi B **224**, 751 (2001).

[41] H. Inoue, N. Ichiroku, T. Torimoto, T. Sakata, H. Mori, and H. Yoneyama, Langmuir **10**, 4517 (1994).

[42] J. Nanda, S. Sapra, and D. D. Sarma, Chem. Mater. **12**, 1018 (2000).

[43] R. Rossetti, R. Hull, J. M. Gibson, and L. E. Brus, J. Chem. Phys. **82**, 552 (1985).

[44] Y. Nakaoka and Y. Nosaka, Langmuir **13**, 708 (1997).

[45] W. Vogel, P. H. Borse, N. Deshmukh, and S. K. Kulkarni, Langmuir **16**, 2032 (2000).

[46] Spin-orbit coupling lifts the sixfold degeneracy into a quartet and a doublet.

[47] In practice, the intervalley mixing between the four equivalent minima at the L point breaks the ideal eightfold degeneracy. The observed splittings decrease with the nanocrystal size (for the nanocrystal of radius 1.1 nm they are of the order of 30 meV).

[48] S. H. Wei and A. Zunger, Phys. Rev. B **49**, 14337 (1994).

[49] We have checked that the sp^3d^5 model is also more sensitive to the passivation of the ZnS/CdS structures. By setting the dangling-bond potential to 100 eV, the energy of the lowest electron state decreases by about 30 meV in the sp^3s^* model and by 50 meV in the sp^3d^5 approach.

[50] L. Thamizhmani, A. K. Azad, J. Dai, and W. Zhang, Appl. Phys. Lett. **86**, 131111 (2005).

[51] R.-H. Xie, G. W. Bryant, S. Lee, and W. Jaskólski, Phys. Rev. B **65**, 235306 (2002).

[52] J.-L. Zhu, S. Zhu, Z. Zhu, Y. Kawazoe, and T. Yao, J. Phys.: Condens. Matter **10**, L583 (1998).